J Therm Anal Calorim (2016) 124:171–180
DOI 10.1007/s10973-015-5130-y

Synthesis and thermal dehydroxylation kinetic of anhydrous calcium phosphate monetite $CaHPO_4$

Raphaèl Mulongo-Masamba[1] · Taoufik El Kassri[1] · Mariam Khachani[1] · Said Arsalane[1] · Mohammed Halim[1] · Adnane El Hamidi[1]

Received: 8 July 2015 / Accepted: 24 October 2015 / Published online: 4 November 2015
© Akadémiai Kiadó, Budapest, Hungary 2015

Abstract In this study, we have synthesized and performed the thermal decomposition kinetics of anhydrous calcium phosphate monetite $CaHPO_4$ under air atmosphere by TG/DTG and DTA techniques using non-isothermal experiments. The prepared and calcined products at 500 °C were characterized by powder X-ray diffraction, infrared spectroscopy, transmission electron microscopy and X-ray microanalysis. The degradation of $CaHPO_4$ was observed between [425–490 °C] and leads to the formation of calcium pyrophosphate by condensation of orthophosphate groups. The kinetic parameter results achieved by the isoconversional methods combined to Malek's procedure showed that the thermal dehydroxylation is a single-step process which related to crystal nucleation and growth mechanism, according to JMA (n) model, with $n = 1.37$ and an activation energy of Friedman $E_\alpha = 299.4 \pm 2.1$ kJ mol^{-1}. The thermodynamic functions (ΔS^*, ΔH^* and ΔG^*) of the thermal dehydroxylation step were calculated using the activated complex theory. The obtained values showed that the reaction is directly related to the introduction of heat and is non-spontaneous process.

Keywords Calcium phosphate · Thermal analysis · Kinetics · Nucleation and growth · Pyrophosphate

✉ Adnane El Hamidi
adnane_el@hotmail.com

[1] Laboratory of Physicochemical of Materials, Catalysis and Environment (CNRST-URAC 26), Faculty of Sciences, University of Mohammed V, Avenue Ibn Battouta, BP 1014, 10000 Rabat, Morocco

Introduction

Ceramics belonging to the family of calcium phosphates constitute an attractive class of compounds rich by their diverse compositions, structures and physico-chemical properties [1, 2]. The large variety of these materials can be distinguished by type of phosphate groups bonded to calcium ions. Among them, calcium orthophosphates like dicalcium phosphate dihydrate $CaHPO_4{\cdot}2H_2O$ (brushite, DCPD), dicalcium phosphate anhydrous $CaHPO_4$ (monetite, DCPA) and calcium pyrophosphate $Ca_2P_2O_7$ (CPP) present biological importance in the formation of bones and teeth at the physiological environment and find practical uses in dental cements and restorative materials [3]. Additionally, due to their chemical stability in acidic media, dicalcium phosphates are used as ion exchangers [4], adsorbents [4–6], and solid electrolytes in battery devices [7]. Recently they received great interest in high technology as luminescent products and sensors [8].

The monetite DCPA is one of the most studied calcium phosphates due to its particular structure and stability [9]. Several methods have been proposed for the synthesis of monetite phosphate in order to get a pure crystalline phase with controlled morphologies [10]. It can be conventionally obtained by dehydration of DCPD phosphate at 250 °C or by methods including wet chemical precipitation, sol–gel synthesis, combustion technique and recently sonochemical process [11, 12]. Nevertheless, wet chemistry methods (sol–gel, precipitation) are preferred as the synthesis way for monetite $CaHPO_4$ due to a series of advantages like the possibility of controlling the final product morphology and phase composition. The calcium phosphate monetite crystallizes at room temperature in a triclinic unit cell with space group $P\overline{1}$, $Z = 4$. Its structure consists of $CaHPO_4$

chains bonded together by Ca–O bonds and three types of hydrogen bonds. Two distinct sets of pairs of PO_4^{3-} units are found in each primitive cell and induce a band splitting [13].

The thermal analysis represents one of convenient way to investigate the thermal stability of materials and determine the kinetic parameters of their conversion process. In this purpose, the conversion of dicalcium phosphate DCPA under various conditions has been the subject of several previous studies, but they are mainly limited to the determination of activation energy [14, 15]. To the best of our knowledge, no complete kinetic description and thermodynamic properties of thermal degradation of monetite phosphate have been reported in the literature. The dicalcium pyrophosphate $Ca_2P_2O_7$ (CPP) can be obtained from monetite (DCPA) by heating in air at the temperature range 325–700 °C. This thermal conversion occurs in a discrete step with an irreversible reaction [15]. The solid-state phase change, monetite to pyrophosphate, was qualified as dehydration–condensation process through abrupt reorganization of phosphorus environment [16] and leads to a poor crystalline phase γ-$Ca_2P_2O_7$ whose crystallographic identity has not been established.

In the present work, we have undertaken the synthesis and thermal behavior of dicalcium phosphate monetite DCPA using simultaneous thermal gravimetric and differential thermal analysis (TG–DTA) in order to determine the kinetic model describing completely the degradation reaction. The purity of synthesized material was controlled by XRD and FTIR analyses. The texture and morphology of particles were examined by TEM–EDS microscopy. The activation energy and reaction model were determined under non-isothermal conditions using isoconversional model-free method and Malek's procedure, respectively. The kinetic parameters were interpreted, and the decomposition mechanism was proposed based on XRD, FTIR and TEM analyses.

Materials and methods

Synthesis

Anhydrous calcium phosphate monetite $CaHPO_4$ was synthesized by the chemical precipitation method using calcium carbonate $CaCO_3$ (calcite) and phosphoric acid (H_3PO_4, 85 % w/w). Both reagents were of analytical grade and used without purification. A stoichiometric solution of $CaCO_3$ and pure H_3PO_4 were separately preheated up at 85 ± 5 °C. H_3PO_4 was then added slowly to $CaCO_3$ suspension under stirring (350 rpm) and the mixture was maintained under reflux at 85 °C, in an oil bath for 24 h. The white precipitate was then filtered, washed several times with hot distilled water, dried overnight at 60 °C, and finally placed in desiccator. Some of the product was calcined at 500 °C overnight for further structural characterization.

Characterization

XRD analysis was carried out to identify and assess phases purity obtained after different calcinations. The diagrams were collected using a Siemens D500 Powder Diffractometer equipped with copper anticathode ($\lambda_{CuK\alpha}$ = 1.541838 Å) at scanning speed of 0.02° s^{-1}. FTIR–ATR characterization of the samples was performed using a Jasco FT/IR 4600 spectrometer equipped with a Jasco ATR PRO ONE module. The samples were scanned in transmission mode with 4 cm^{-1} resolution at the range 4000–400 cm^{-1}. TEM–EDS micrographs were obtained with a Tecnai G2 (FEI Company) operating at 120 kV with 0.35 nm resolution and equipped with EDS microanalyzer. The simultaneous TG/DTG/DTA analyses were carried out on a Labsys™ Evo (1F) Setaram apparatus. ICTAC kinetics committee recommendations for collecting experimental data [17] and performing kinetics computations [18] were followed to evaluate the kinetic parameters. Before analysis, the thermal analysis system was firstly calibrated for temperature reading with reference metals of 99.99 % purity. It was also essential to calibrate the balance for buoyancy effects to allow quantitative estimation of mass changes. The experiments were conducted under non-isothermal conditions in air flow atmosphere of 30 mL min^{-1} from room temperature up to 800 °C, at various heating rates (5, 10, 15 and 20 °C min^{-1}). The measurements were repeated three times in order to ensure the reproducibility. An initial mass of sample of about 5.0 ± 0.1 mg was placed in an alumina pan. The sample was well dispersed with negligible depth to minimize heat and mass transfers.

Kinetic study

The kinetic analysis of thermal decomposition in solid-state reactions is based on the transformation rate equation expressed as follows:

$$\frac{d\alpha}{dt} = A \ \exp\left(\frac{-E}{RT}\right) f(\alpha) \quad (1)$$

where A is the pre-exponential (frequency) factor, E is the activation energy of the reaction, T is the absolute temperature, R is the gas constant, $f(\alpha)$ is the reaction model that gives information about mechanism of the reaction, and α is the conversion degree. In thermogravimetry, α is defined as:

$$\alpha = \frac{m_0 - m_t}{m_0 - m_\infty} \tag{2}$$

where, m_0 is initial mass, m_t is mass at time t, and m_∞ is final mass.

The determination of each parameter of Eq. (1) (A, E and $f(\alpha)$) can be done using the model-free computational method, which is considered more accurate especially for detecting complicated processes occurring at different ranges of temperature [18, 19]. This approach is based on the isoconversional principle which states that the reaction rate at constant conversion degree depends only on temperature [20]. It allows for evaluating the Arrhenius parameters without prior knowledge of the reaction model, but requires a minimum of three heating rates.

Determination of the activation energy E_α

The differential isoconversional method suggested by Friedman [21] is derived from Eq. (1) and it is based on the following equation:

$$\ln\left[\left(\frac{d\alpha}{dt}\right)_{\alpha,\beta}\right] = \ln[Af(\alpha)] - E_\alpha/RT_{\alpha,\beta} \tag{3}$$

The apparent activation energy (E_α) is determined from the slope of the plot of $\ln[(d\alpha/dt)_{\alpha,\beta}]$ versus $1/T_{\alpha,\beta}$, at a constant α value. Compared to other existing methods, Friedman's procedure is rather accurate because it does not include any forms of numerical approximations.

The Ozawa–Flynn–Wall (OFW) method is an integral method that evaluates the temperature integral using the Doyle's approximation [22]. From Eq. (1), we obtain the derived function:

$$g(\alpha) = \int_0^\alpha \frac{1}{f(\alpha)} d\alpha \tag{4}$$

that becomes as follows:

$$g(\alpha) = \frac{AE}{R\beta}\left[\frac{\exp(-x)}{x} - \int_x^\infty \left(\frac{\exp(-x)}{x}\right) dx\right] = \frac{AE}{R\beta} p(x) \tag{5}$$

where $x = E/RT$ is the reduced apparent activation energy, $p(x)$ is a temperature integral function and β is the heating rate. Hence, OFW equation [23] is expressed:

$$\ln \beta = Cste - 1.05\frac{E_\alpha}{RT_{\alpha,\beta}} \tag{6}$$

Kissinger, Akahira and Sunose (KAS) used the approximation given by Coats and Redfern [24] to estimate the temperature integral. KAS equation is expressed as follows:

$$\ln\left(\frac{\beta}{T^2_{\alpha,\beta}}\right) = Cste - \frac{E_\alpha}{RT_{\alpha,\beta}} \tag{7}$$

where $Cste$ is a constant.

Determination of reaction model

In thermal analysis, the reaction model $f(\alpha)$ is a theoretical and mathematical description of the progress of process that may provide information about the mechanism. In order to find the most suitable reaction model of the investigated process, the Malek's method [25] was considered. With the knowledge of activation energy and if it is almost constant, it can be replaced by an average apparent value E_α. A pair of special functions $y(\alpha)$ and $z(\alpha)$ can then be calculated using the Eqs. (8) and (9) below:

$$y(\alpha) = \frac{d\alpha}{dt} \times \exp\left(\frac{E_\alpha}{RT}\right) \tag{8}$$

$$z(\alpha) = p(x) \times \left(\frac{d\alpha}{dt}\right) \times \frac{T}{\beta} \approx T^2 \times \left(\frac{d\alpha}{dt}\right) \tag{9}$$

where x is the reduced apparent activation energy (E_α/RT), $p(x)$ may be accurately estimated by means of the fourth rational expression of Senum and Yang [26] and later on corrected by Flynn [27]:

$$p(x) = \left(\frac{e^{-x}}{x}\right)\frac{x^3 + 18x^2 + 86x + 96}{x^4 + 20x^3 + 120x^2 + 240x + 120} \tag{10}$$

The $y(\alpha)$ and $z(\alpha)$ maxima (α_m and α_p^∞, respectively) allow to determine the appropriate reaction model in accordance with the conditions defined by Malek's procedure [25] (Table 1).

Thermodynamic parameters

The activated complex theory was used by many authors to determine the thermodynamic parameters involved during thermal decomposition of organic and inorganic materials [28]. Based on the theory developed by Eyring [29], the thermodynamic functions may be calculated according to the following equations:

$$\Delta S^* = R \cdot \ln\left(\frac{A \cdot h}{e \cdot \chi \cdot k_B \cdot T_{p,0}}\right) \tag{11}$$

$$\Delta H^* = E^* - R \cdot T_{p,0} \tag{12}$$

$$\Delta G^* = \Delta H^* - T_{p,0} \cdot \Delta S^* \tag{13}$$

where A is the pre-exponential factor, h is the Planck constant, $e = 2.7183$ is the Neper number, χ is the transition factor, which is equal to unity for monomolecular reactions, k_B is the Boltzmann constant, $T_{p,0}$ is the

Table 1 Mathematical expressions for different reaction models and their mechanistic significances

Reaction model	Symbol	$f(\alpha)$	$y(\alpha)$	$z(\alpha)$
Reaction nth order model (nucleation/decay)	F_n/RO	$(1-\alpha)^n$	$n < 1$: Convex $n > 1$: Concave	α_p^∞ depends on exponents
Phase boundary controlled reaction (contracting area, i.e., bidimensional shape or one-half order kinetics)	R_2	$2(1-\alpha)^{1/2}$	Convex	0.750
Phase boundary controlled reaction (contracting area, i.e., tridimensional shape or two-thirds order kinetics)	R_3	$3(1-\alpha)^{2/3}$	Convex	0.704
Johnson–Mehl–Avrami general equation (growth of nuclei)	JMA (n)	$n(1-\alpha)[-\ln(1-\alpha)]^{1-1/n}$	$n < 1$: Concave $n = 1$: Linear $n > 1$: Maximum	0.632
One dimensional diffusion	D_1	$1/2\alpha$		
Two dimensional diffusion	D_2	$-1/\ln(1-\alpha)$	Concave	0.834
Three dimensional diffusion (Jander's equation)	D_3	$\frac{3(1-\alpha)^{2/3}}{2\left[1-(1-\alpha)^{1/3}\right]}$	Concave	0.704
Three dimensional diffusion (Ginstling equation)	D_4	$\frac{3}{2\left[(1-\alpha)^{-1/3}-1\right]}$	Concave	0.776
Sestak Breggren (autocatalytic model)	SB (m, n)	$f(\alpha) = (\alpha)^m (1-\alpha)^n$		α_p^∞ depends on exponents

maximum peak temperature in DTA curves and E^* is the apparent activation energy E_α.

The value of peak temperature $T_{p,0}$ corresponds to the temperature taken from an equilibrium state. Because the heat lag of the process depends on the heating rate, the smaller is the heating rate, the smaller is the peak shift to higher temperatures, which indicates that the equilibrium state corresponds to $\beta \to 0$, and it is obtained from the Eq. (14) [30].

$$T_{p,i} = T_{p0} + a \cdot \beta_i + b \cdot \beta_i^2 \quad (14)$$

where a and b are constants.

Results and discussion

XRD analysis

X-ray powder diffraction patterns of the as-prepared calcium phosphate DCPA and its calcined form at 500 °C are shown in Fig. 1. The diffractogram of untreated sample (Fig. 1a) reveals almost all characteristic diffraction peaks corresponding to $CaHPO_4$ with a structure comparable to the standard data (JCPDS No. 9-80). The XRD pattern of the annealed compound (Fig. 1b) presents a poor crystalline phase characteristic to γ form of calcium pyrophosphate (γ-$Ca_2P_2O_7$) with standard data (JCPDS No. 17-499). The obtained results are consistent with those reported in previous works [14].

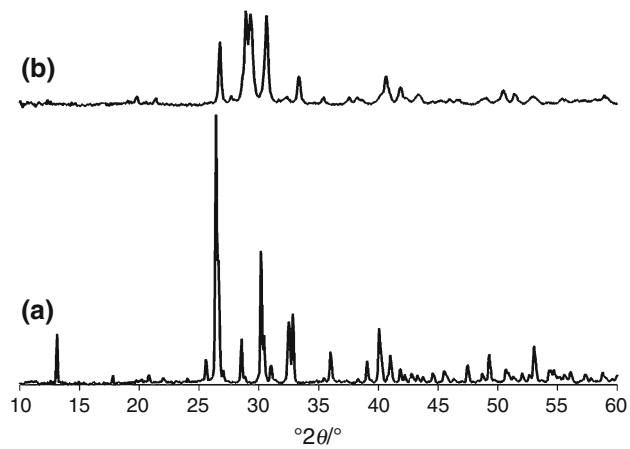

Fig. 1 XRD patterns of *a* calcium phosphate DCPA and *b* its calcined form at 500 °C

FTIR–ATR spectroscopy

The FTIR–ATR spectra of DCPA and its calcined form at 500 °C are displayed in Fig. 2. The multiple bands observed in the regions 1200–400 cm^{-1} (Fig. 2a) can be assigned to internal vibration modes of P–O in $CaHPO_4$. The strong vibration bands at 1123, 1054 and 987 cm^{-1} and the shoulder at 1180 cm^{-1} are attributed to stretching vibrations of the P–O band, while the band at 881 cm^{-1} is related to stretching vibration of the acidic phosphate group P–O(H). The observed bands at 554, 520 and 405 cm^{-1} are assigned to the O–P–O deformations. The vibrational

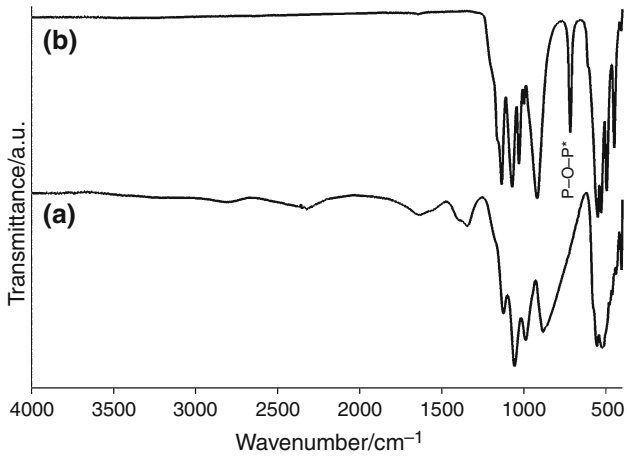

Fig. 2 FTIR–ATR patterns of *a* calcium phosphate DCPA and *b* its annealed form at 500 °C

bands related to the acidic hydrogen of $CaHPO_4$ are observed at 1644 cm^{-1} for bending vibrations and at 2327, 2810 and 3210 cm^{-1} for the stretching vibrations [31]. These latter bands have been assigned to three types of hydrogen bonds in $CaHPO_4$ [31]. Dehydration of the compound (Fig. 2b) induced the formation of pyrophosphate $Ca_2P_2O_7$ with its characteristic sharp band at 717 cm^{-1} assigned to the stretching mode of the P–O–P bridges typically observed in pyrophosphates.

TEM–EDS analysis

Transmission electron microscopy (TEM) results of calcium phosphate DCPA and its calcined form are displayed in Fig. 3. The particles of the as-prepared DCPA show similar plate-like crystals with dimensions ranging from 1 to 2 µm (Fig. 3a). After calcination at 500 °C, the particles became rod shaped with an average size of about 25 nm in diameter and vary in length from 20 to 100 nm (Fig. 3b). The nanoparticulate shape of the material gives also evidence to the broadness of its XRD peaks displayed in Fig. 1. The calcium/phosphorus molar ratio determined by chemical microanalysis (EDS) was found to be stoichiometric and equal to 1, both for $CaHPO_4$ and calcium pyrophosphate $Ca_2P_2O_7$ (Table 2).

Thermal analysis

The non-isothermal decomposition of calcium phosphate DCPA was carried out at 10 °C min^{-1} under flowing air atmosphere. The typical TG, DTG and DTA curves are presented in Fig. 4.

According to thermal analysis measurements, the decomposition of dicalcium phosphate monetite DCPA occurs in one step in the range of temperature between 400 and 500 °C, with a maximum DTG at 464 °C. The observed mass loss was about 6.55 %, which is very close to the theoretical value of 6.61 %, corresponding to removal of 0.5 mol of H_2O. The DTA scan of the decomposition reaction displays an endothermic effect centered at 467 °C. This result shows that the thermal decomposition reaction of $CaHPO_4$ involves an intramolecular dehydration of the deprotonated hydrogen phosphate groups (HPO_4^{2-}) and induces the formation of γ-$Ca_2P_2O_7$. The decomposition process is formally represented as:

$$2CaHPO_4 \longrightarrow \gamma\text{-}Ca_2P_2O_7 + H_2O \quad (15)$$

Indeed, the XRD and FTIR results (Figs. 1b, 2b) show a beginning of crystallization of calcium pyrophosphate γ-$Ca_2P_2O_7$, after decomposition reaction. This behavior is frequently observed in thermal transformations of orthophosphates to pyrophosphates, which occurs by condensation of PO_4^{3-} groups to $P_2O_7^{4-}$.

At higher temperature of about 730 °C, calcium pyrophosphate γ-$Ca_2P_2O_7$ is transformed to allotropic form β-$Ca_2P_2O_7$ as was observed in previous papers [14].

Kinetic study

In order to obtain a reliable kinetic data of the decomposition process of calcium phosphate DCPA, a series of dynamic scans were used with multiple temperature programs ($\beta = 5$, 10, 15 and 20 °C min^{-1}). The obtained conversion degree α and reaction rate $d\alpha/dt$ curves (Fig. 5) at different heating rates have the same shape, characterized by an almost asymmetric behavior, and moves to higher temperature when increasing the heating rate. This is due to the acceleration of variations in the rate of heat transfer with increasing heating rate and the decrease of exposure time at a particular temperature at higher heating rates. It can also be explained by the temperature gradient inside and outside the particles, which is lower at lower heating rate [17].

Model-free estimation of activation energy E_α

According to the basic kinetic concepts, the determination of activation energies at different conversion degrees α can provide valuable information about the complexity of reaction mechanism. For this purpose, three isoconversional methods were used: the differential analysis of Friedman (FR), and the integral analyses of Ozawa–Flynn–Wall (OFW) and Kissinger–Akahira–Sunose (KAS). The

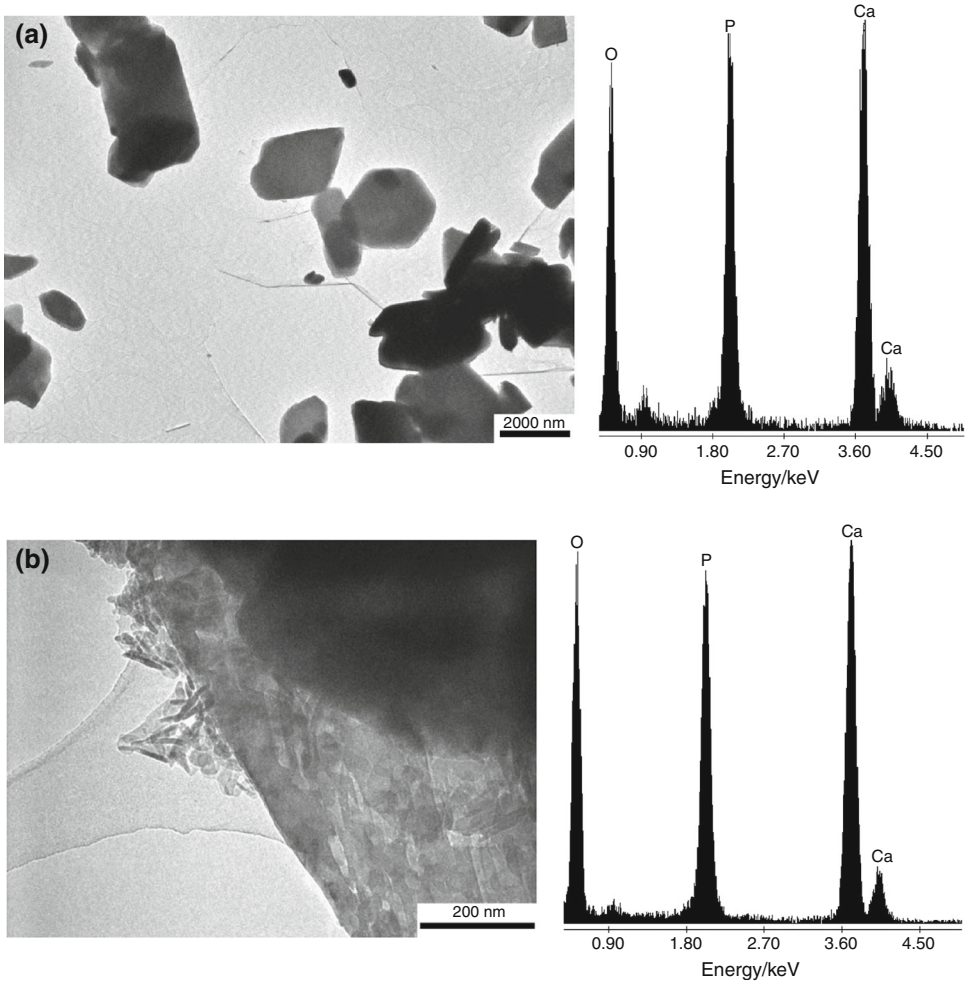

Fig. 3 TEM–EDS analysis of **a** calcium phosphate DCPA and **b** its calcined form at 500 °C

Table 2 EDS analysis of calcium phosphate DCPA and its calcined form at 500 °C

Ca/P molar ratio	DCPA	CPP
EDS analysis	0.93–1.03	0.98–1.05

activation energies were calculated under a range of α between 0.05 and 0.95 with a step of 0.05 (Fig. 6).

The dependency of the activation energy with conversion degree "$E_\alpha = f(\alpha)$" is observed similar for the three applied methods (Fig. 6). Some changes may be expected for lower and higher values of α. This is probably due to the errors generated by the temperature integral approximation or in the baseline interpolation for peak tails [32, 33]. The values displayed show an almost constant shape in the α range [0.2–0.8], which indicates that the decomposition mechanism of calcium phosphate DCPA can be fairly regarded as a single-step process. In what follow, we have considered the activation energy calculated by the Friedman's method whose average value is $E_\alpha = 299.4 \pm 2.1$ kJ mol^{-1}.

Determination of reaction model

Malek's methodology

In order to find the kinetic model of thermal dehydroxylation of calcium phosphate DCPA, the special functions $y(\alpha)$ and $z(\alpha)$ were calculated from Eqs. (8) and (9), respectively, and normalized within [0, 1] interval. The variation of these functions with conversion degree is displayed in Fig. 7.

For all heating rates, the shapes of $y(\alpha)$ and $z(\alpha)$ plots are identical and confirm the single-step decomposition process of calcium phosphate DCPA. The conversion values corresponding to the maxima of $y(\alpha)$ and $z(\alpha)$ plots, α_m and α_p^∞, respectively, are listed in Table 3. The displayed average maxima are $\alpha_m = 0.244$ and $\alpha_p^\infty = 0.610$.

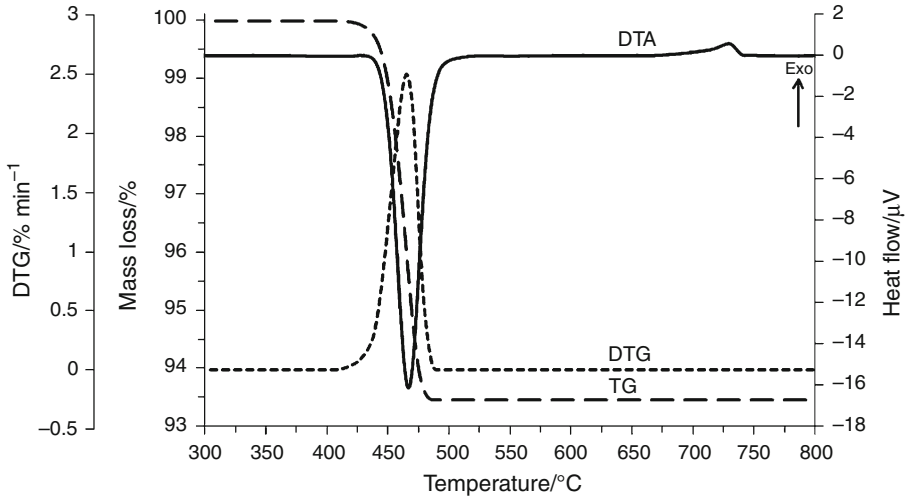

Fig. 4 Thermal decomposition curves of calcium phosphate DCPA at 10 °C min^{-1}

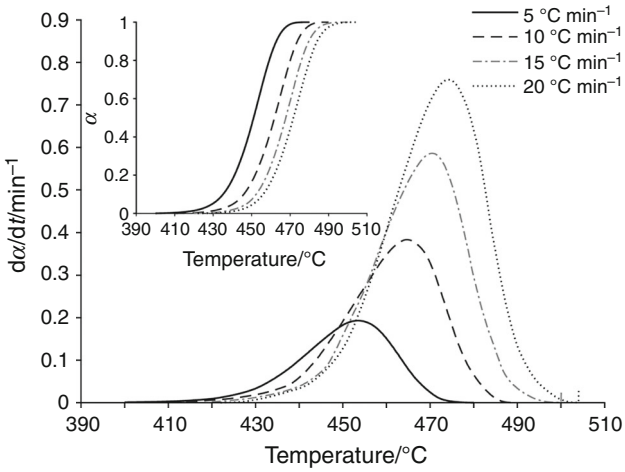

Fig. 5 TG and DTG curves of thermal decomposition of DCPA at different heating rates

According to Malek's procedure, if the maximum falls into $0.61 \leq \alpha_p^{\infty} \leq 0.65$, the Johnson–Mehl–Avrami (JMA (n)) model represents the best choice to describe the investigated process. Its $f(\alpha)$ function can be expressed as:

$$f(\alpha) = n(1-\alpha)[-\ln(1-\alpha)]^{1-1/n} \tag{16}$$

where n is the kinetic exponent.

In order to ascertain the chosen model, the linearity of the double logarithmic plot of $\ln[-\ln(1-\alpha))]$ as a function of $1/T$, introduced by Satava [17], was tested. The obtained results, displayed in Fig. 8, are clearly linear with a correlation coefficient greater than 0.99 (Table 4).

The mathematical modeling of the experimental results was carried out by nonlinear regression using the error function (S), $S = \sum_1^N \left(y_i^{exp} - y_i^{the}\right)^2$. The obtained kinetic parameters and the simulated curves at different

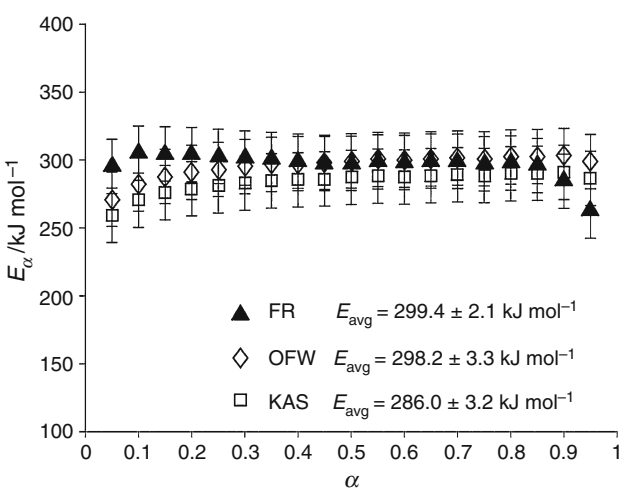

Fig. 6 The variation of activation energy E_α versus conversion degree α using three different methods

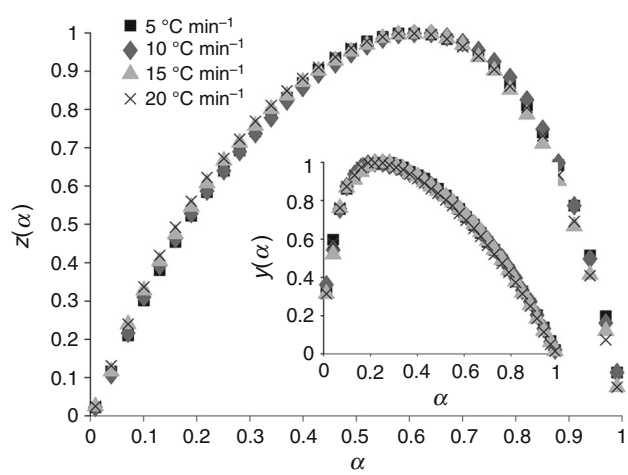

Fig. 7 Variation of $y(\alpha)$ and $z(\alpha)$ as function of conversion degree α at different heating rates

heating rates are summarized in Table 5 and Fig. 9, respectively.

The JMA parameters thus obtained may indicate a combination between 1- and 2-dimensional nucleation and growth mechanism, which is in close relation with the rod-shaped particles observed by TEM analysis. The mechanism of nucleation and growth was already reported for the decomposition and dehydration of various solids [34, 35]. The found mechanism and observed decrease in particle size occur more probably in three steps as was reported previously [34]. The decomposition of calcium phosphate $CaHPO_4$ can be estimated as a reaction interface process that begins with destruction of the reactant crystalline phase of $CaHPO_4$ and its structural rearrangement, followed by the instantaneous diffusion of the generated water molecules toward the surface. Afterward, the concomitant formation of rod particles of γ-$Ca_2P_2O_7$ takes place by the elimination of gaseous H_2O through a bulk nucleation and growth mechanism. This possible mechanism was confirmed by XRD, FTIR and TEM analyses.

Thermodynamic parameters

The thermodynamic parameters ΔS^*, ΔH^* and ΔG^* were calculated using the Eqs. (11)–(13), based on the values of average apparent activation energy E_α of Friedman, pre-exponential factor A obtained by Malek's procedure and the temperature at maximum peak $T_{p,0} = 440.94$ °C calculated from Eq. (14). The obtained parameters are summarized in Table 6.

The positive value of activation entropy ΔS^* means that the activated complex has lower degree of arrangement than the initial solid. This increasing disorder is in accordance with the decrease of crystallinity observed by XRD analysis. On the other hand, the positive value of the activated enthalpy ΔH^* confirms the endothermic nature of the process as was observed by DTA analysis. The positive value of the free Gibbs energy ΔG^* shows that the thermal dehydroxylation of calcium phosphate $CaHPO_4$ is non-spontaneous process and needs heat to occur under atmosphere pressure.

Table 3 Values of α_m, α_p and α_p^∞ at different heating rates and their corresponding standard deviations (SD)

β/ °C min^{-1}	α_m	α_p	α_p^∞
5	0.252	0.592	0.602
10	0.244	0.605	0.613
15	0.247	0.613	0.623
20	0.234	0.596	0.603
Average	0.244	0.601	0.610
SD	0.009	0.006	0.006

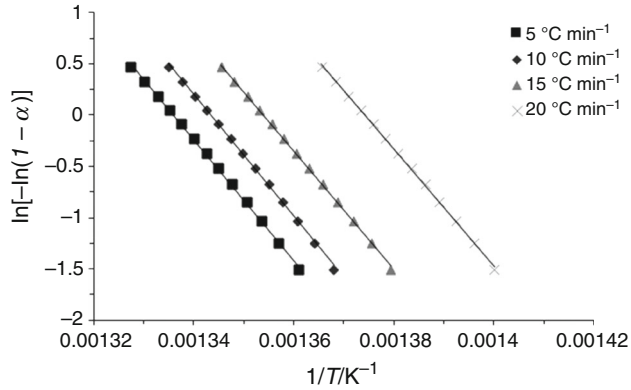

Fig. 8 Test of applicability of the JMA model

Table 4 Parameters of the double logarithm plot

β/ °C min^{-1}	5	10	15	20
n	1.59	1.61	1.66	1.63
R^2	0.9996	0.9997	0.9993	0.9993

Table 5 Kinetic parameters obtained using JMA (n) model and their corresponding standard deviations (SD)

β/ °C min^{-1}	ln$A$	n	R^2
5	48.5	1.39	0.9995
10	48.4	1.40	0.9994
15	48.5	1.35	0.9992
20	48.5	1.33	0.9990
Average	48.5	1.37	
SD	0.034	0.028	

Conclusions

Thermal decomposition kinetics of anhydrous calcium phosphate $CaHPO_4$ to calcium pyrophosphate γ-$Ca_2P_2O_7$ has been investigated from a series of analytical experiments at different constant heating rates. The kinetic parameters and the appropriate reaction model were established by applying the isoconversional model-free method and Malek's procedure. The variation of activation energy E_α was found constant, which reveals a single-step reaction mechanism. The application of the Malek's kinetic

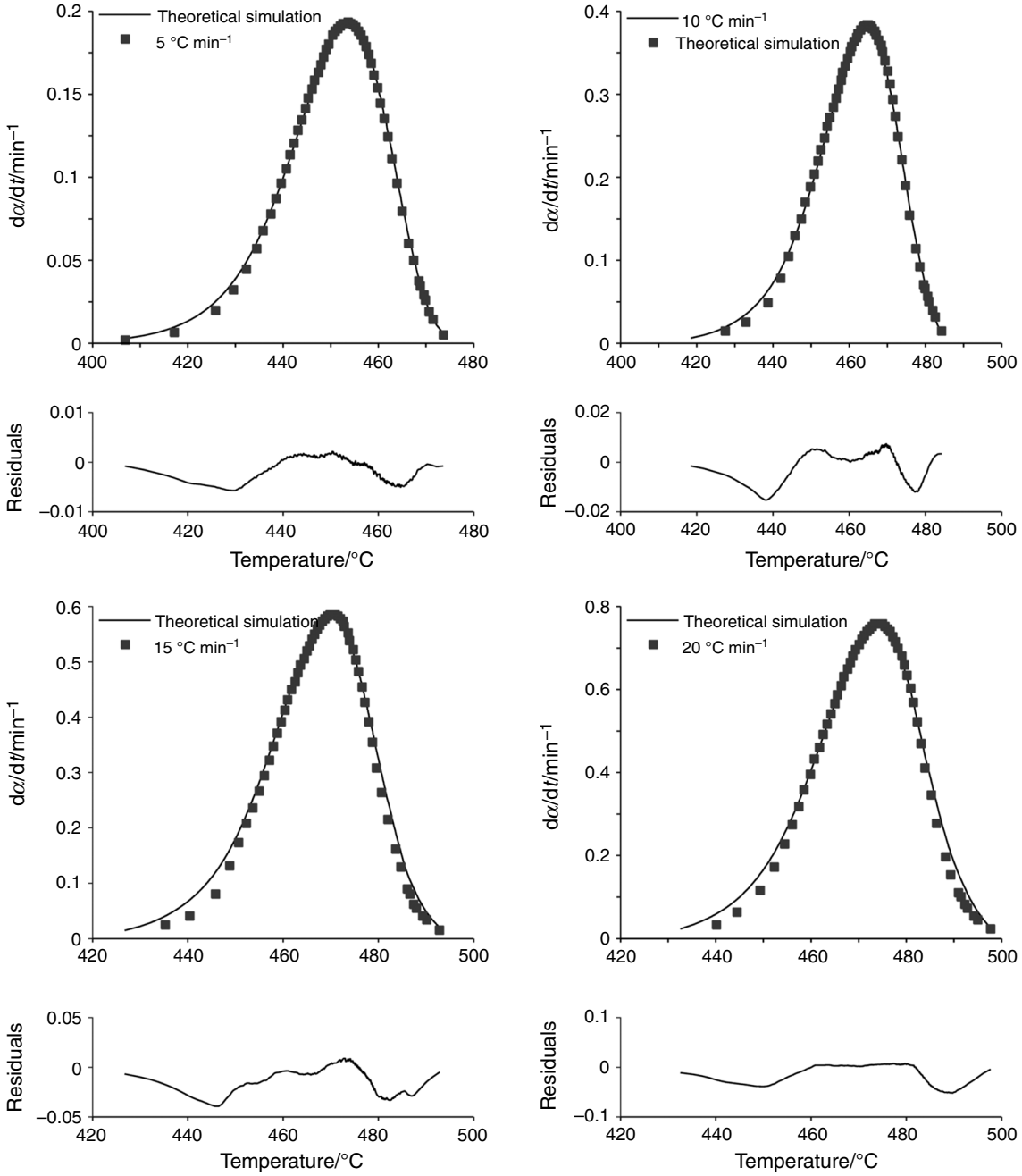

Fig. 9 Simulated kinetic curves at different heating rates and their residuals plotted underneath

Table 6 Thermodynamic parameters of thermal decomposition of calcium phosphate DCPA

ΔS^*/J mol^{-1} K^{-1}	ΔH^*/kJ mol^{-1}	ΔG^*/kJ mol^{-1}
179.3	292.1	164.0

procedure suggested the Johnson–Mehl–Avrami model (JMA), relative to a nucleation and growth mechanism of the dehydroxylation reaction. The deduced dehydroxylation mechanism of dicalcium phosphate $CaHPO_4$ is considered as an interface reaction process that begins with

destruction of the reactant crystalline structure followed by the diffusion and removal of the gaseous water molecules to form the rod-shaped particles of γ-$Ca_2P_2O_7$, through a complex 1-dimensional/2-dimensional bulk nucleation and growth mechanism, controlled by the kinetic model equation $f(\alpha) = 1.37(1 - \alpha)[-\ln(1 - \alpha)]^{(1-1/1.37)}$. The values of apparent activation energy E, pre-exponential factor A, as well as the changes of entropy, enthalpy and Gibbs free energy for the formation of activated complex gave certain conclusions concerning the mechanism and characteristics of the process.

Acknowledgements This research was financially supported by University of Mohammed V - Morocco under the Project No. SCH 04/09 and CNRST-Morocco.

References

1. Dorozhkin SV. Calcium orthophosphates. J Mater Sci. 2007;42:1061–95.
2. Dorozhkin SV. Calcium orthophosphates in nature, biology and medicine. Materials. 2009;2:399–498.
3. Dorozhkin SV. Calcium orthophosphates: occurence, properties, biomineralization, pathological calcification and biomimetic applications. Biomaterials. 2011;1:121–64.
4. El Hamidi A, Mulongo Masamba R, Khachani M, Halim M, Arsalane S. Kinetics modeling in liquid phase sorption of copper ions on brushite di-calcium phosphate di-hydrate $CaHPO_4{\cdot}2H_2O$ (DCPD). Desalin Water Treat. 2015;56:779–91.
5. Da Silva Filho EC, da Silva OG, da Fonseca MG, Arakaki LNH, Airoldi C. Synthesis and thermal characterization of copper and calcium mixed phosphates. J Therm Anal Calorim. 2007;87: 775–8.
6. Da Silva OG, da Fonseca MG, Arakaki LNH. Silylated calcium phosphates and their new behavior for copper retention from aqueous solution. Colloid Surf A. 2007;301:376–81.
7. Tortet L, Gavarri JR, Nihoul G, Dianoux AJ. Study of protonic mobility in $CaHPO_4{\cdot}2H_2O$ (Brushite) and $CaHPO_4$ (Monetite) by infrared spectroscopy and neutron scattering. J Solid State Chem. 1997;132:6–16.
8. Doat A, Pellé F, Lebugle A. Europium-doped calcium pyrophosphates: allotropic forms and photoluminescent properties. J Solid State Chem. 2005;178:2354–62.
9. Miyazaki T, Sivaprakasam K, Tantry J, Suryanarayanan R. Physical characterization of dibasic calcium phosphate dihydrate and anhydrate. J Pharm Sci. 2009;98:905–16.
10. Chen GG, Luo GS, Yang LM, Xu JH, Sun Y, Wang JD. Synthesis and size control of $CaHPO_4$ particles in a two-liquid phase micromixing process. J Cryst Growth. 2005;279:501–7.
11. Eshtiagh H, Houssaindokht MR, Chahkandhi M, Youssefi A. Preparation of anhydrous dicalcium phosphate, DCPA, through sol–gel process, identification and phase transformation evaluation. J Non-Cryst Solids. 2008;354:3854–7.
12. Baradaran S, Basirun WJ, Mahmoudian M, Hamdi M, Alias Y. Synthesis and characterization of monetite prepared using a sonochemical method in a mixed solvent system of water/ethylene glycol/*N*,*N*-dimethylformamide. Metall Mater Trans A. 2013;44:2231–8.
13. Dickens B, Bowen JS, Brown WE. A refinement of the crystal structure of $CaHPO_4$ (synthetic monetite). Acta Crystallogr B Struct Sci. 1972;28:797–806.
14. Wikholm NW, Beebe RA, Kittelberger JS. Kinetics of the conversion of monetite to calcium pyrophosphate. J Phys Chem. 1975;79:853–6.
15. Berend G, Hegedüs AJ. Thermoanalytical investigation of secondary calcium phosphate dehydrate. Thermochim Acta. 1975; 11:367–79.
16. Hlel F, Kamoun S, Guidara K. Investigation of phosphorus site condensation in $CaHPO_4$ by analysis of ^{31}P MAS–NMR tensor and X-ray powder patterns. Z Naturforsch A. 2006;61:375–82.
17. Vyazovkin S, Chrissafis K, Di Lorenzo ML, Koga N, Pijolat M, Roduit B, Sbirrazzuoli N, Suñol JJ. ICTAC kinetics committee recommendations for collecting experimental thermal analysis data for kinetic computations. Thermochim Acta. 2014;590:1–23.
18. Vyazovkin S, Burnham AK, Criado JM, Pérez-Maqueda LA, Popescu C, Sbirrazzuoli N. ICTAC kinetics committee recommendations for performing kinetic computations on thermal analysis data. Thermochim Acta. 2011;520:1–19.
19. Sbirrazzuoli N, Vincent L, Bouillard J, Elégant L. Isothermal and non-isothermal kinetics when mechanistic information available. J Therm Anal Calorim. 1999;56:783–92.
20. Brown ME, Gallagher PK. Handbook of thermal analysis and calorimetry: recent advances, techniques and applications. 1st ed. Amsterdam: Elsevier; 2008.
21. Friedman HL. Kinetics of thermal degradation of char-forming plastics from thermogravimetry. Application to a phenolic plastic. J Polym Sci Polym Symp. 1964;6:183–95.
22. Doyle CD. Estimating isothermal life from thermogravimetric data. J Appl Polym Sci. 1962;6:639–42.
23. Ozawa T. A new method of analyzing thermogravimetric data. Bull Chem Soc Jpn. 1965;38:1881–6.
24. Coats AW, Redfern JP. Kinetic parameters from thermogravimetric data. Nature. 1964;201:68–9.
25. Málek J. The kinetic analysis of non-isothermal data. Thermochim Acta. 1992;200:257–69.
26. Senum GI, Yang RT. Rational approximations of the integral of the Arrhenius function. J Therm Anal. 1977;11:445–7.
27. Flynn JH. The "temperature integral"—its use and abuse. Thermochim Acta. 1997;300:83–92.
28. Shannon RD. Activated complex theory applied to the thermal decomposition of solids. Trans Faraday Soc. 1964;60:1902–13.
29. Eyring H. The activated complex in chemical reactions. J Chem Phys. 1935;3:107–15.
30. Ma H, Yan B, Li J, Ren Y, Chen Y, Zhao F, Song J, Hu R. Molecular structure, thermal behavior and adiabatic time-to-explosion of 3,3-dinitroazetidinium picrate. J Mol Struct. 2010;981: 103–10.
31. Petrov I, Šoptrajanov B, Fuson N, Lawson JR. Infra-red investigation of dicalcium phosphates. Spectrochim Acta A Mol Spectrosc. 1967;23:2637–46.
32. Šimon P, Thomas P, Dubaj T, Cibulková Z, Peller A, Veverka M. The mathematical incorrectness of the integral isoconversional methods in case of variable activation energy and the consequences. J Therm Anal Calorim. 2013;115:853–9.
33. Sbirrazzuoli N, Vincent L, Mija A, Guigo N. Integral, differential and advanced isoconversional methods: complex mechanisms and isothermal predicted conversion–time curves. Chemometr Intell Lab. 2009;96:219–26.
34. Koga N, Tanaka H. A physico-geometric approach to the kinetics of solid-state reactions as exemplified by the thermal dehydration and decomposition of inorganic solids. Thermochim Acta. 2002;388:41–61.
35. Koga N, Takemoto S, Tatsuya N, Haruhiko T. A kinetic study of the thermal decomposition of iron(III) oxide-hydroxides. Part 3. Shape control and thermal decomposition of α-FeO(OH). Thermochim Acta. 1996;282(283):81–90.